ARTICLE

Principles of visual cortex excitatory microcircuit organization

Christina Y.C. Chou,[1,2] Hovy H.W. Wong,[1,3] Connie Guo,[1,2] Kiminou E. Boukoulou,[1] Cleo Huang,[1] Javid Jannat,[1] Tal Klimenko,[1] Vivian Y. Li,[1] Tasha A. Liang,[1] Vivian C. Wu,[1] and P. Jesper Sjöström[1,*]
*Correspondence: jesper.sjostrom@mcgill.ca

Received: December 25, 2023; Accepted: November 13, 2024; Published Online: December 12, 2024; https://doi.org/10.1016/j.xinn.2024.100735

GRAPHICAL ABSTRACT

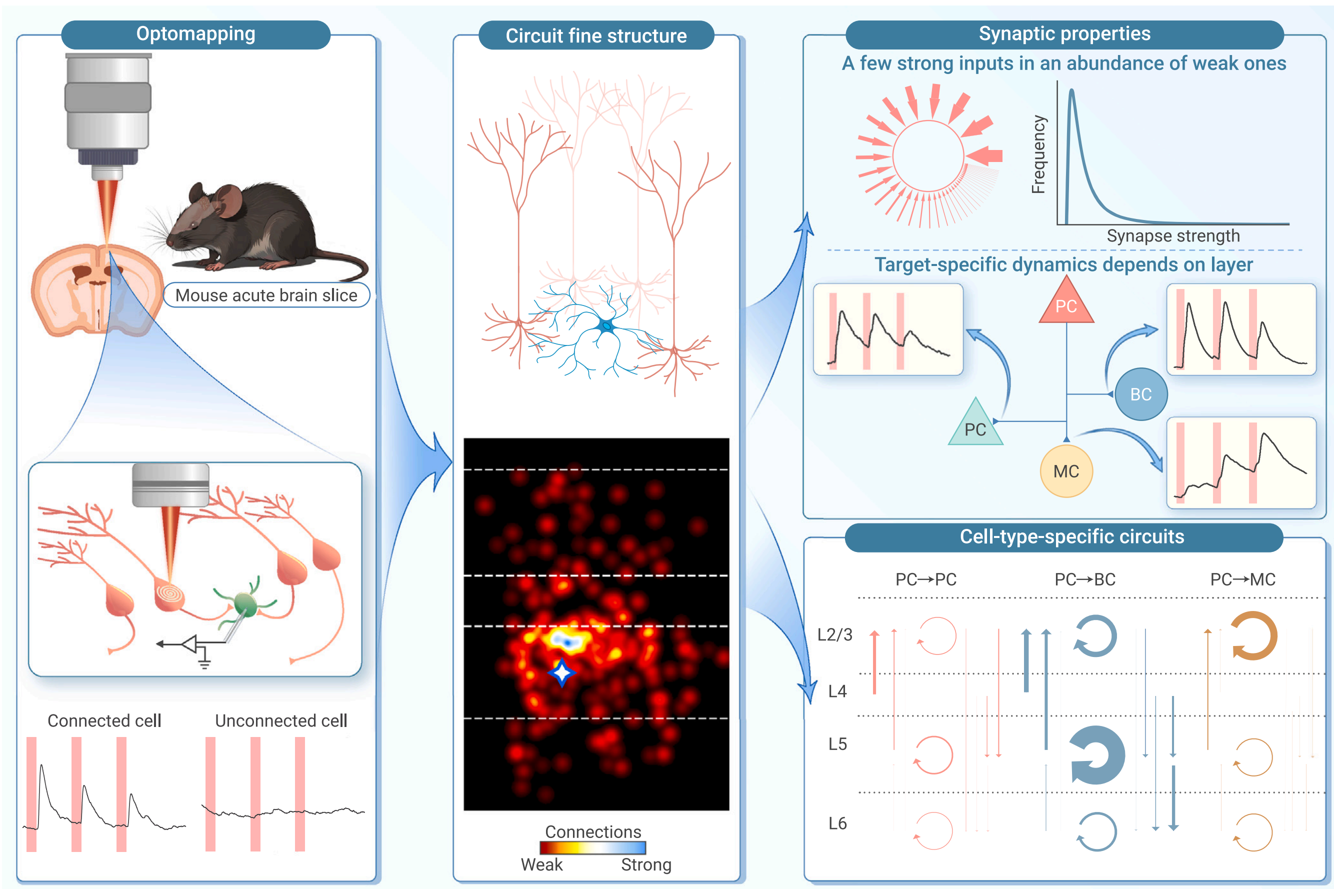

PUBLIC SUMMARY

- Optomapping is a fast two-photon optogenetic technique that charts brain microcircuits at ~100 times the speed of traditional patching methods.
- In mouse visual cortex, optomapping verified canonical pyramidal circuits but found surprising excitation patterns in basket and Martinotti cells, concentrated in layers 5 and 2/3.
- Excitatory inputs distribute log normally, with a handful of strong synapses among mostly weaker ones, extending this principle from excitatory to inhibitory neurons.
- Short-term synaptic changes that influence information transfer surprisingly depend on cortical layer in addition to target cell.
- This work sheds light on cortical circuit structure and synaptic dynamics, offering a faster approach to mapping microcircuits at synaptic resolution.

Principles of visual cortex excitatory microcircuit organization

Christina Y.C. Chou,[1,2] Hovy H.W. Wong,[1,3] Connie Guo,[1,2] Kiminou E. Boukoulou,[1] Cleo Huang,[1] Javid Jannat,[1] Tal Klimenko,[1] Vivian Y. Li,[1] Tasha A. Liang,[1] Vivian C. Wu,[1] and P. Jesper Sjöström[1,*]

[1]Centre for Research in Neuroscience, Brain Repair and Integrative Neuroscience Program, Department of Neurology and Neurosurgery, The Research Institute of the McGill University Health Centre, Montreal, QC H3G 1A4, Canada

[2]Integrated Program in Neuroscience, McGill University, Montreal, QC H3A 2B4, Canada

[3]Present address: Gerald Choa Neuroscience Institute, School of Biomedical Sciences, The Chinese University of Hong Kong, Hong Kong, China

*Correspondence: jesper.sjostrom@mcgill.ca

Received: December 25, 2023; Accepted: November 13, 2024; Published Online: December 12, 2024; https://doi.org/10.1016/j.xinn.2024.100735

Citation: Chou C.Y.C., Wong H.H.W., Guo C., et al., (2025). Principles of visual cortex excitatory microcircuit organization. The Innovation **6(1)**, 100735.

Synapse-specific connectivity and dynamics determine microcircuit function but are challenging to explore with classic paired recordings due to their low throughput. We therefore implemented optomapping, a ~100-fold faster two-photon optogenetic method. In mouse primary visual cortex (V1), we optomapped 30,454 candidate inputs to reveal 1,790 excitatory inputs to pyramidal, basket, and Martinotti cells. Across these cell types, log-normal distribution of synaptic efficacies emerged as a principle. For pyramidal cells, optomapping reproduced the canonical circuit but unexpectedly uncovered that the excitation of basket cells concentrated to layer 5 and that of Martinotti cells dominated in layer 2/3. The excitation of basket cells was stronger and reached farther than the excitation of pyramidal cells, which may promote stability. Short-term plasticity surprisingly depended on cortical layer in addition to target cell. Finally, optomapping revealed an overrepresentation of shared inputs for interconnected layer-6 pyramidal cells. Thus, by resolving the throughput problem, optomapping uncovered hitherto unappreciated principles of V1 structure.

INTRODUCTION

Information processing in the brain is determined by patterns of synaptic connectivity and short-term plasticity.[1–3] Classically, canonical circuits are organized as columnar pathways across cortical layers.[4–6] However, there is a relative paucity of information on connectivity and short-term plasticity with target-cell specificity.[7–9]

Yet, the rules that govern plasticity and connectivity patterns are specific to synapse type.[7-9] For instance, the same neocortical pyramidal cell (PC) axon produces short-term depressing or facilitating synapses depending on target cell type.[10,11] Synapse-type-specific patterning is anticipated, as different neuronal classes play distinct functional roles, e.g., mediating excitation or inhibition.[12–14]

Cortical microcircuits are furthermore populated by recurring inhibitory connectivity motifs. For instance, basket cells (BCs)[12–14] mediate fast-onset perisomatic inhibition of PCs,[15] whereas Martinotti cells (MCs)[12–14] provide slow-onset inhibition of PC apical dendrites.[15,16] BCs and MCs thereby critically determine PC computations.

Cortical connections must thus be explored with synapse-type specificity,[7–9] which has long been achieved with multiple patch-clamp recordings. In rodent primary visual cortex (V1) networks, multiple patch has revealed, e.g., non-random fine structure,[17] functional specificity,[18,19] and excitatory/inhibitory specificity,[20,21] even with human comparison.[20]

Multiple patch, however, suffers from sampling shortcomings since results are gathered across cells, acute slices, and animals.[17,18,20–22] Findings may thus arise from pooling data across experiments. For example, high-order connectivity patterns are deduced by sampling across paired recordings.[17,23,24] Similarly, log-normal distribution of synaptic weights[17,25] may emerge as an artifact of cross-cell sampling, which is important since log normality has been linked to functions such as feature preference.[18,19]

Furthermore, because multiple patch is prohibitively slow, it is generally not feasible to measure connectivity or plasticity across the entire thickness of a given cortical area, which has limited what kinds of queries neuroscientists can explore. There has thus been a long-standing need for synapse-specific approaches with considerably higher throughput.[7,26]

Two-photon (2P) optogenetics, which can reliably activate individual neurons with high spatiotemporal precision,[27–33] is a promising approach for resolving the throughput problem. Several studies that combine 2P optogenetics with patch-clamp electrophysiology have achieved high-resolution optogenetic circuit mapping.[29,34–40]

Here, we devised and validated a 2P optogenetic high-throughput circuit charting approach, which we called optomapping. We optomapped connectivity, synaptic weights, and short-term dynamics of excitatory synapses onto PCs, BCs, and MCs across the layers of mouse V1, which revealed striking and surprising target-cell-specific differences. Our findings provide a fresh perspective on the principles that govern V1 excitatory fine structure.

RESULTS

Reliable optogenetic activation of candidate input cells

Through neonatal viral injection[41] in Emx1$^{Cre/Cre}$ mice,[42] we targeted ChroME opsin and mRuby[33] to PC somata while simultaneously tagging interneurons with GFP[43] (supplemental materials and methods; Figures 1A and 1B). We activated PCs with 1,040-nm 2P spiral scans (Figures S1A and S1B),[27] which reliably evoked spiking up to ~70 Hz (Figures S1C and S1D). Surplus spiking was indistinguishable from current injection, spike latency was ~5 ms, and jitter was <0.5 ms (Figures S1E–S1I), similar to classical current clamp. Spike-probability half-widths at half-maximum ($w_{1/2}$) was ~5 μm laterally and ~13 μm axially (Figures S1J and S1K), as inherited from the 2P excitation resolution (Figure S2). The $w_{1/2}$ was smaller than the ~20-μm distance between ChroME-expressing PCs (see supplemental materials and methods). In conclusion, we could, with 2P optogenetics, reliably drive spiking with single-cell resolution and millisecond temporal precision (Figure S1), as previously shown.[27,29,30,33,34,37,38,40,44]

Sample optogenetic synaptic connectivity map

To map connectivity, we patched a PC, BC, and/or MC and sequentially spiral scanned mRuby3-positive PCs in a field of view (FOV; Figures 1C–1E). To avoid dissection artifacts, we optomapped ~100 μm into slices cut normal to the pial surface (Figure S3). We verified that the detection of connections was robust (Figures S3H and S3I). While recording the same postsynaptic cell, adjacent FOVs were subsequently optogenetically stimulated (Figure 1F).

In offline analysis, presynaptic PCs that statistically elicited excitatory postsynaptic potentials (EPSPs) in the patched cell were semi-automatically tagged as connected (Figure 1C). EPSP amplitude was used as a metric of connective strength, and the paired-pulse ratio (PPR) quantified short-term plasticity. To enable comparison of connectivity and synaptic strength across cortical layers, we assigned a 200-μm-wide vertical column centered on the postsynaptic cell as well as layer boundaries based on standard layer-specific features (see supplemental materials and methods).[45–47]

In this sample experiment, the high throughput of optomapping allowed us to probe 363 candidate presynaptic PCs, of which 35 were connected (Figure 1G). For comparison, this throughput over a whole-cell recording lasting 1–2 h is ~100-fold faster than multiple patch-clamp recordings, depending on the specific comparison.[17,18,20–22] To enable averaging of connectivity maps across different postsynaptic cells of the same type, we created synaptic input density maps (Figure 1H; see supplemental materials and methods). For context, such maps cannot be meaningfully created for paired recordings.

From this individual map, we observed that, although this layer 2/3 (L2/3) BC received appreciable within-layer excitation as previously reported,[20,48] cross-layer excitation from L4 and L5 was substantial, revealing a high success rate at finding connections hundreds of μm from the patched cell. Laterally in L2/3, connectivity qualitatively died down over tens to hundreds of μm (Figures 1G

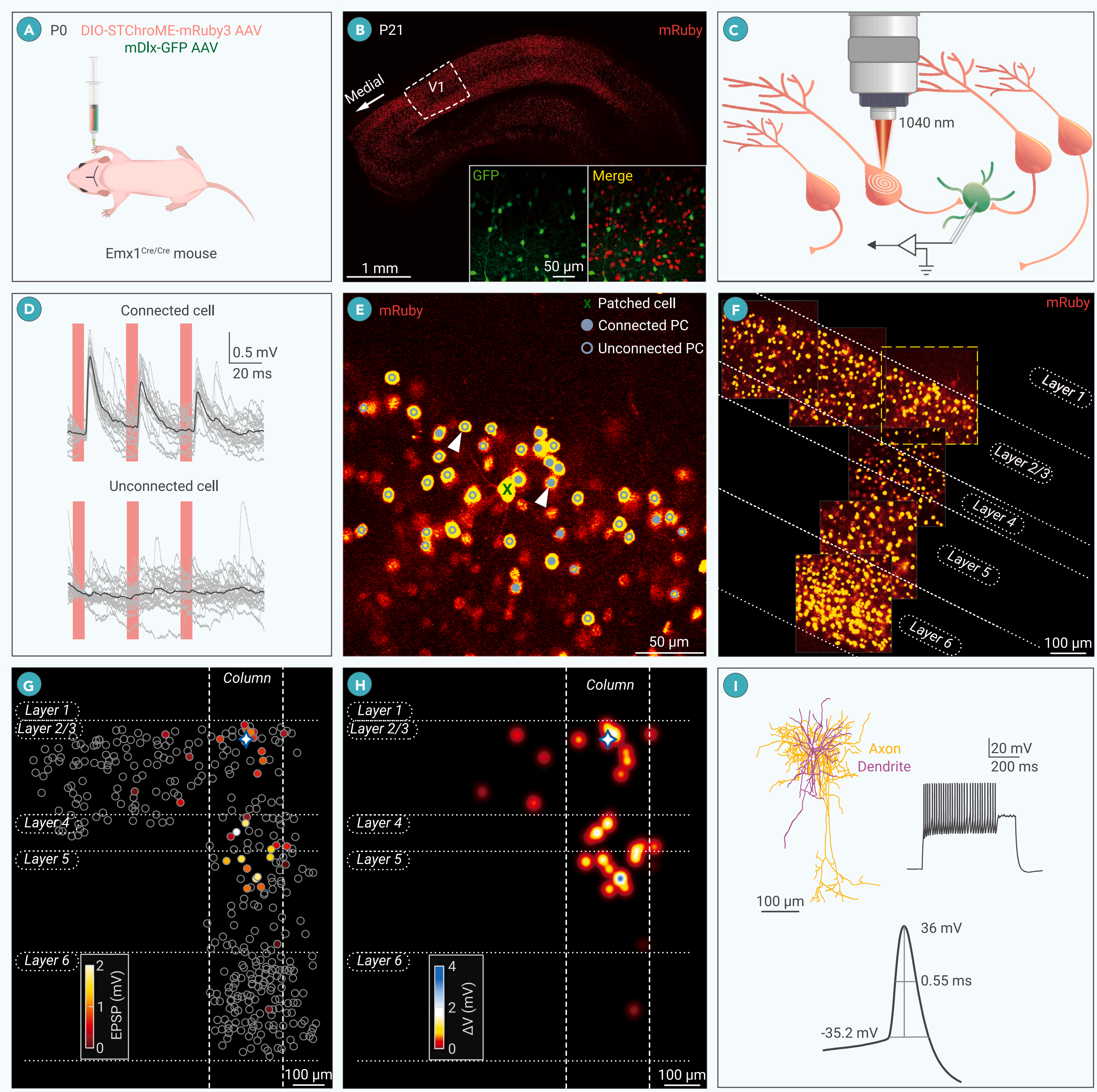

Figure 1. Sample optomap of excitatory inputs onto an individual cell (A and B) Viral injection in Emx1$^{Cre/Cre}$ neonates[41,42] targeted ChroME and mRuby to PC somata[33] and GFP to interneurons,[43] shown at postnatal day (P)21. (C) We spiral scanned mRuby-positive PCs with a 2P laser beam while whole-cell recording a postsynaptic cell, here a GFP-expressing interneuron. (D) Statistical detection across 20 sweeps (gray) determined connectivity, with mean sweep (black) determining synaptic efficacy and dynamics (see supplemental materials and methods). (E) Sample FOV with PCs eliciting EPSPs (closed circles) or not (open circles) in recorded L2/3 cell (green X). Arrowheads: samples in (D). (F) By repeating (E) across adjacent FOVs, the cortical thickness as well as hundreds of μm laterally were mapped. Yellow dash: FOV in (E). (G) Input PCs are color coded by EPSP amplitude (circles) elicited in patched cell (diamond). The column (dotted lines) enables comparison across patched cells. (H) Synaptic input density map of (G) enables averaging across patched cells (diamond; see main text). (I) Patched sample cell was morpho-electrophysiologically classified as BC (see supplemental materials and methods).

and 1H).[20,48] Detailed statistical comparisons across different postsynaptic cells of these observations are provided below.

Accounting for optogenetic stimulation artifacts

Emx1$^{Cre/Cre}$ mice drive expression in >90% of excitatory neurons.[42,49] Consequently, we occasionally directly depolarized patched PCs when spiral scanning nearby presynaptic PCs. Compared to EPSPs, direct depolarization was instantaneous, had a small coefficient of variation (CV), and had no short-term dynamics (Figure S4). Direct depolarization only occurred within ~60 μm of the patched PC (Figures S4E–S3H). We thus relied on a combination of patched cell type (PC vs. BC/MC), onset latency, stimulation location, CV, and short-term dynamics to determine if a location elicited direct depolarization (Figures S4B–S4I), which we then accounted for (Figure S4J; supplemental materials and methods).

In conclusion, for a negligible fraction of proximal PC→PC connections, synaptic weight and dynamics might be distorted. Since Emx1-Cre does not target inhibitory cells,[42,49] this artifact did not affect PC→BC or PC→MC optomapping.

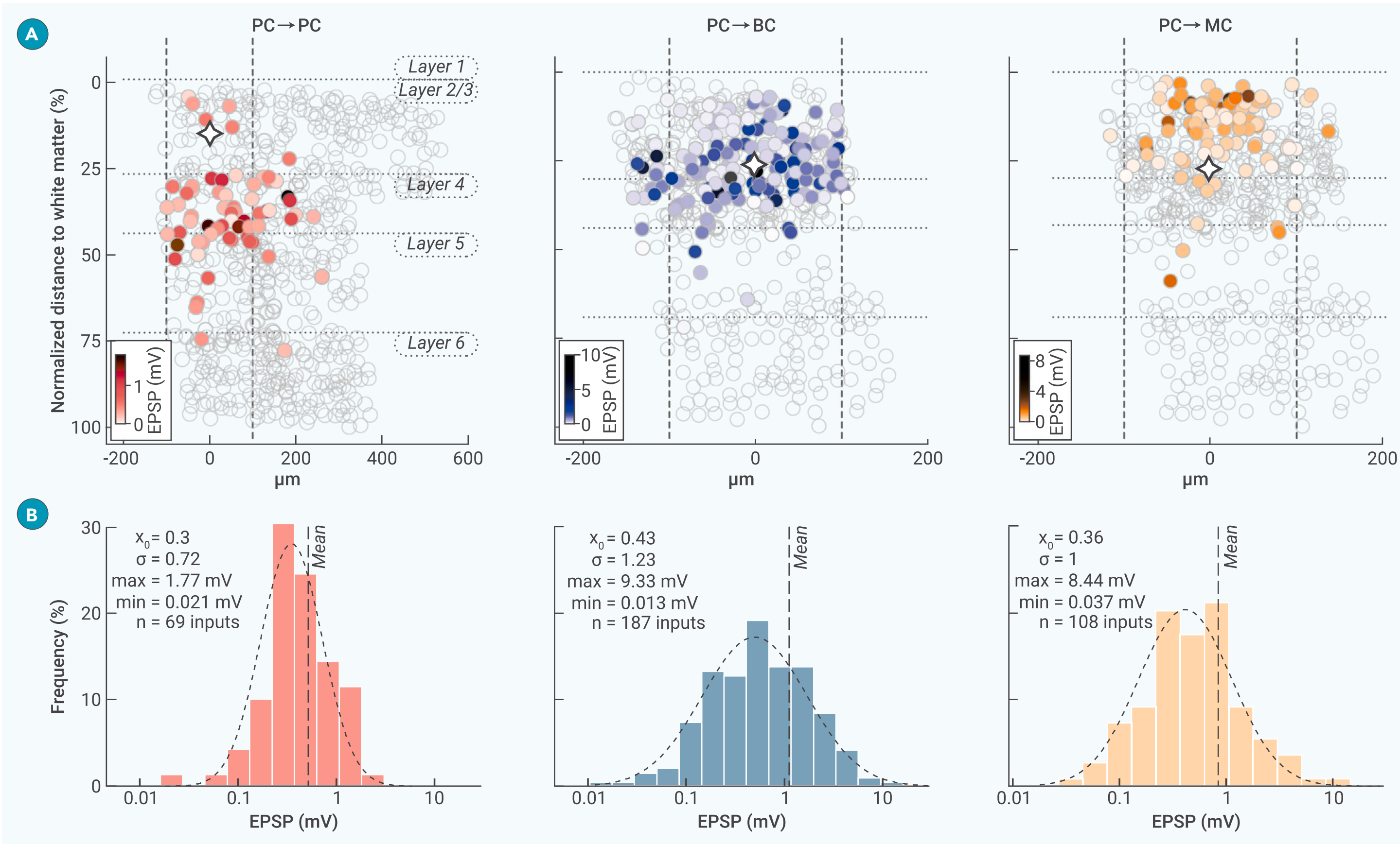

Figure 2. EPSPs in individual L2/3 cells distribute log normally (A) We explored the distribution of synaptic weights in a single L2/3 PC, BC, and MC. Open circles: unconnected presynaptic neurons. Closed circles: connected presynaptic neurons. Diamond: patched postsynaptic cell. (B) EPSP distributions from cells in (A) were best fit by a log-normal model (see supplemental materials and methods). Dashed line: mean EPSP amplitude. Dotted line: log-normal fit.

Identification of PCs, BCs, and MCs

It is known that synaptic connectivity, weight, and short-term dynamics depend on the target cell.[7–9] We therefore hierarchically clustered patched cells[50] into PCs, BCs, and MCs based on morphology and electrophysiology (Figures 1I, S5, and S6; see supplemental materials and methods). PC, BC, and MC properties matched prior descriptions,[12–14] suggesting accurate classification.

Excitatory synaptic strengths distribute log normally

Previous paired-recording studies found log-normal synaptic strength distributions, but the data were pooled across cells and days.[17,19,22,51] We therefore asked if synaptic weights onto individual L2/3 cells also distributed log normally (Figure 2A). We found that the best-fit distribution type was log normal for individual PCs, BCs, and MCs (Figure 2B). EPSP amplitudes pooled across PCs, BCs, and MCs also distributed log normally (Figure S7). Although means and standard deviations differed across PCs, BCs, and MCs, the best-fit distribution model did not. From this emerged the principle that excitatory synaptic weights distribute log normally regardless of target cell type.

In L2/3, PCs and BCs receive a strong ascending drive, while that of MCs is local

Due to the slow throughput of classic paired patch, it has been challenging to explore how synaptic connectivity distributes spatially.[48,52] We therefore optomapped the spatial input distributions for PCs, BCs, and MCs, starting in L2/3, which revealed strikingly different connectivity patterns (Figure 3A).

Consistent with the canonical circuit,[4–6,53] L2/3 PCs received more inputs from L4 than from other layers (Figures 3A and 3B). L5 PC→L2/3 PC connectivity was also high, as previously reported.[34] L6 PC→L2/3 PC connectivity was low. Similar to L2/3 PCs, L2/3 BCs received many excitatory inputs from L2/3, L4, and L5 but few from L6 (Figures 3A and 3B). In contrast, L2/3 MCs received the most input from the same layer (Figure 3A), more so than L2/3 PCs did. L2/3 MCs also received more inputs from L5 than from L4 (Figures 3A and 3B). L4 PC→L2/3 MC connectivity was lower than that of L4 PC→L2/3 BCs and L4 PC→L2/3 PCs. L6→L2/3 excitatory connections were strikingly rare for all three cell types (Figures 3A and 3B).

We optomapped hundreds of microns laterally, but excitatory inputs were chiefly detected within 300 μm (Figure 3A), in keeping with prior literature.[20,48] However, the excitation of BCs seemingly originated farther away (see below for details). We observed no mediolateral asymmetries.

To compare synaptic strengths, we relied on the amplitude of the first EPSP in a train of three EPSPs (Figure 1D). Input strengths were indistinguishable across layers except for L2/3 BCs, where L6 inputs were weaker (Figure 3C). Excitatory inputs were stronger onto L2/3 BCs than onto L2/3 PCs and MCs (Figures 3A and 3C). These comparisons, however, did not account for the strong short-term facilitation of PC→MC connections,[10,11,45,54] which is revisited separately below.

In sum, we revealed target-cell-specific spatial distributions of excitation in L2/3. We found more potent overall excitation of BCs, strong ascending excitation of PCs and BCs but not MCs, and a relatively disconnected L6.[20]

In L5, most excitatory inputs originate from L5

We next explored spatial distributions of excitatory inputs to L5. Here, BCs received more intralaminar inputs than L5 PCs and L5 MCs (Figures 4A and 4B). Connectivity was low for L6→L5, despite these layers being adjacent. Like in L2/3, connection strength depended on input layer for BCs but not PCs or MCs (Figure 4C). Inputs from L4 and L5 were stronger onto L5 BCs than PCs or MCs. Interestingly, PC→BC strength concentrated to upper L5 (Figure 4A).

Overall, spatial distributions were similar across L5 target cell types, chiefly originating from L5. Like L2/3 (Figure 3), the excitation of BCs was stronger than that of PCs or MCs, and L6 was relatively disconnected.[20]

In L6, excitatory inputs are chiefly intralaminar

Next, we investigated the spatial distribution of excitatory connections to L6. L6 PCs and MCs received more excitation from L6 than from other layers,

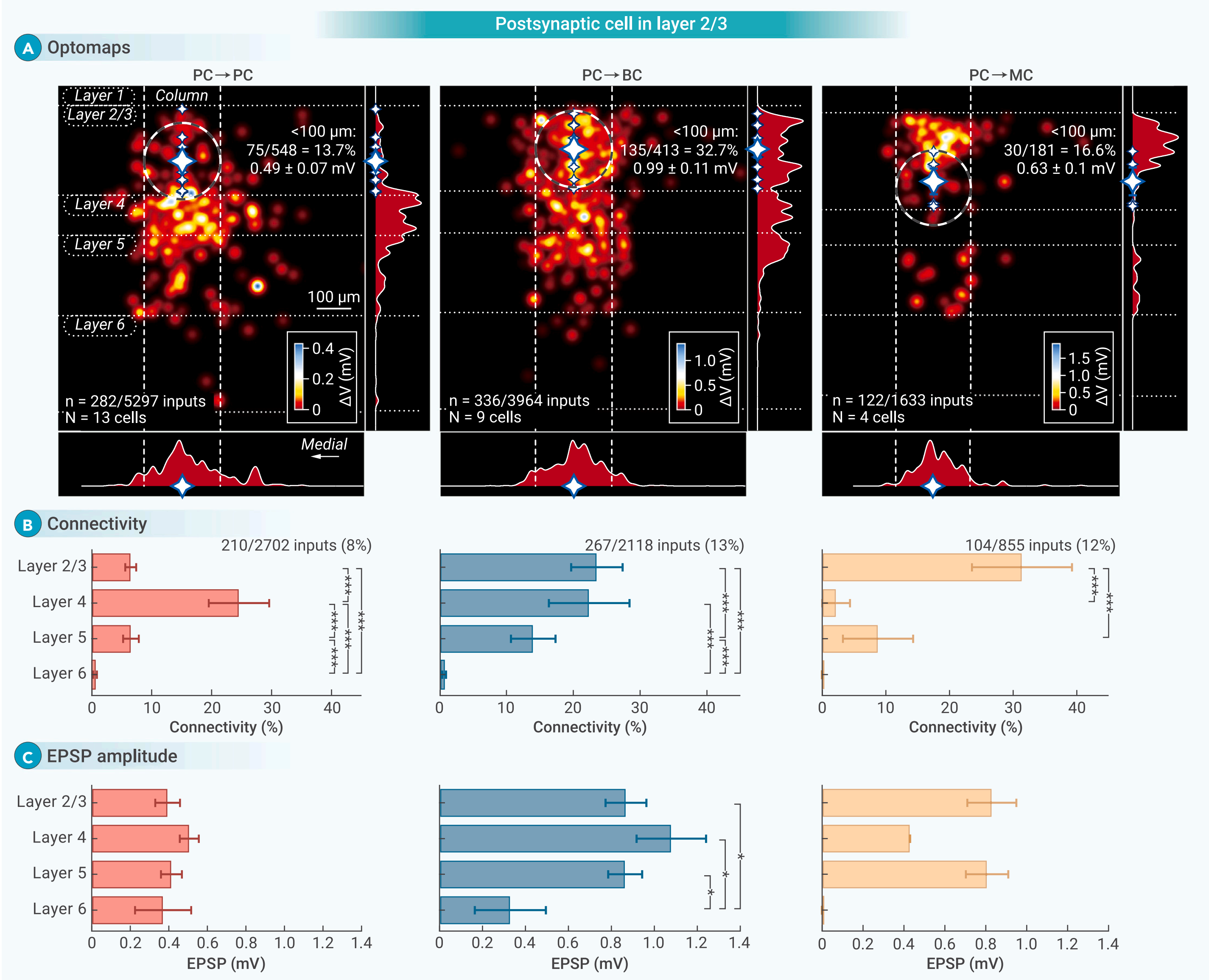

Figure 3. In L2/3, strong ascending PC→PC/BC drive but local PC→MC excitation (A) Synaptic input density maps for L2/3 PCs, BCs, and MCs were generated by averaging individual maps (Figure 1H). Connectivity within a 100-μm radius (dashed circle) enables comparison with paired recordings, which are typically close.[48] Inset right and bottom: vertical and horizontal density projections. Dashed horizontal lines: layer boundaries. Dotted lines: vertical column. (B) L2/3 PCs had higher excitatory connectivity from L4 than from other layers and lower excitatory connectivity from L6. L2/3 BCs had higher excitatory connectivity from L2/3 and L4. L2/3 MCs, on the other hand, had higher excitatory connectivity from L2/3 than from other layers, with few L4 and L6 inputs.[39] L2/3 PCs were more frequently connected to L2/3 BCs and L2/3 MCs than to L2/3 PCs (PC vs. BC, $p < 0.001$; PC vs. MC, $p < 0.001$), L4 PCs were less frequently connected to L2/3 MCs than to L2/3 PCs and L2/3 BCs (PC vs. MC, $p < 0.001$; BC vs. MC, $p < 0.001$), and L5 PCs were more frequently connected to L2/3 BCs than to L2/3 PCs ($p < 0.05$), whereas for L6 inputs, we found no differences. We used generalized linear mixed model (GLMM) statistics (see supplemental materials and methods, presynaptic layer and cell type interaction effect, $p < 0.001$). Numbers: within-column connectivity. Sample sizes: see Table S1. (C) L2/3 PCs received weaker excitatory inputs than L2/3 BCs ($p < 0.01$), regardless of presynaptic layer. MCs, however, were indistinguishable (PC vs. MC, $p = 0.15$; BC vs. MC, $p = 0.99$). LMM statistics revealed that EPSP amplitudes depended on cell type ($p < 0.01$) but not presynaptic layer ($p = 0.12$, interaction effect $p = 0.74$). Mean ± SEM. *$p < 0.05$, **$p < 0.01$, and ***$p < 0.001$.

although L5 PC→L6 BC and L6 PC→L6 BC connectivity rates were indistinguishable (Figures 5A and 5B). L6 BCs also had higher connectivity rates from L5 than L6 PCs or L6 MCs. Within each cell type in L6, there was no difference in connection strength between different layers (Figure 5C), but across cell types in L6, excitatory inputs onto BCs were stronger than excitatory inputs onto PCs and MCs.

In sum, spatial distributions were similar across L6 target cells. Like for L2/3 and L5 (Figures 3 and 4), the excitation of BCs was stronger than that of PCs or MCs, and L6 was isolated.

Excitation of inhibition originates farther away

Qualitatively, the excitation of inhibitory cells (E→I) seemed to originate farther away (Figures 3, 4, and 5). We therefore quantified the spatial decay of connectivity, which indeed revealed more distal E→I than E→E inputs (Figure S8). This E→I/E→E difference could promote stability and difference-of-Gaussian connectivity.

Optomapping and paired patch yield indistinguishable results

To validate optomapping, we compared it with our L5 paired-recording data.[45] One caveat, however, is that our paired-recording study was carried out at a younger age range (paired recordings, postnatal day [P]11–P20: 16 ± 0.1 days, n = 223 vs. optomapping, P17–P25: 21 ± 0.3 days, n = 41, $p < 0.001$, Wilcoxon-Mann-Whitney). Another is that paired-recording studies of the same brain region have been known to disagree,[20,21] meaning this method is not a gold standard.

Our paired recordings were done with cells spaced as closely as possible, meaning <100 μm apart.[17] To enable comparison, we restricted the optomapping dataset to a 100-μm radius of patched cells (Figure 4A, dashed circles).

In L5, PC→PC connectivity rates measured with paired recordings[45] (81/682 = ~11.9%) and optomapping (16.9%; Figure 4A) were indistinguishable (p = 0.055, chi-squared test). However, EPSP amplitude was larger with paired recordings (0.87 ± 0.09 mV, n = 162) than with optomapping (0.33 ± 0.03 mV, n = 59,

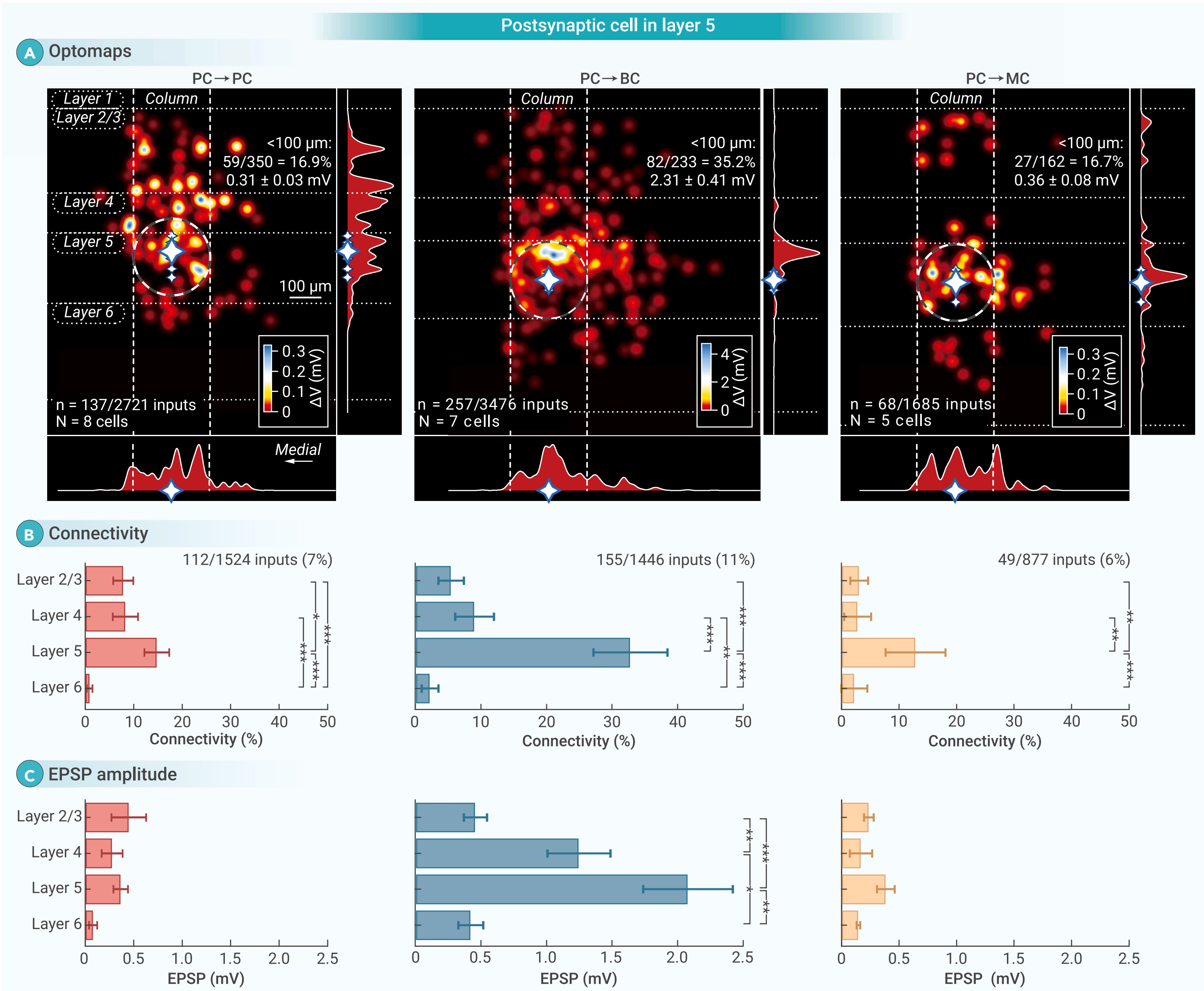

Figure 4. For PCs, BCs, and MCs in L5, excitatory drive concentrated to L5 (A) Synaptic input density maps for L5 PCs, BCs, and MCs. (B) L5 PCs, BCs, and MCs had higher connectivity from L5 than from L2/3 or L6. Within L5, BCs received more excitatory inputs than PCs ($p < 0.001$) or MCs ($p < 0.01$). Connectivity depended on presynaptic layer and cell type ($p < 0.001$). (C) Input strengths onto L5 PCs and MCs did not differ by layer. L5 PC→L5 BC and L4 PC→L5 BC inputs were stronger than inputs from other layers. Inputs from L4 and L5 were stronger onto BCs than onto PCs and MCs (from L4, PCs vs. BCs, $p < 0.05$, BCs vs. MCs, $p < 0.05$; from L5, PCs vs. BCs, $p < 0.01$, BCs vs. MCs, $p < 0.01$). EPSP amplitudes depended on both cell type and presynaptic layer ($p < 0.01$). Mean ± SEM. *$p < 0.05$, **$p < 0.01$, and *** $p < 0.001$.

$p < 0.001$, Wilcoxon-Mann-Whitney). However, the smaller optomapping amplitude agreed with paired recordings from older mice.[20]

For L5 PC→L5 BC synapses, connectivity rates with paired recordings[45] (100/299 = ~33.4%) and optomapping (35.2%; Figure 4A) were indistinguishable ($p = 0.67$, chi-squared test), as were EPSP amplitudes (paired recordings, 2.1 ± 0.2 mV, $n = 100$ vs. optomapping, 2.3 ± 0.4 mV, $n = 82$, $p = 0.66$, Wilcoxon-Mann-Whitney). Likewise, for L5 PC→L5 MC synapses, connectivity rates with paired recordings (4/47 = ~8.5%) and optomapping (16.7%; Figure 4A) were indistinguishable ($p = 0.17$, chi-squared test), as were EPSP amplitudes (paired recordings, 0.21 ± 0.1 mV, $n = 4$ vs. optomapping, 0.36 ± 0.08 mV, $n = 27$, $p = 0.44$, Wilcoxon-Mann-Whitney).

We next directly compared paired patch and optomapping (Figure S9). We optomapped an FOV to find connected PCs. We reasoned that if optomapping worked reliably, then targeting those same PCs for patching should invariably yield connected pairs, which turned out to be true (Figures S9A–S9C). EPSP amplitude and synaptic dynamics were furthermore indistinguishable (Figures S9D–S9F).

In conclusion, as strength differences for L5 PC→PC synapses could be attributed to age,[55] we found no systematic differences. Results obtained with the two methods were thus indistinguishable.

Excitatory pathway structure depends on target cell type

Based on ensemble optomaps (Figures 3, 4, and 5 and associated statistics), we constructed connectivity matrices for PCs, BCs, and MCs (Figure 6A). This highlighted several features, e.g., a prominent L4→L2/3 pathway for PCs (Figure 3), as expected for V1.[4-6,53] In L5, BCs received more excitatory inputs than PCs and MCs (Figure 4). Finally, L2/3 MCs had higher excitatory connectivity from L2/3 than from other layers (Figure 3).

We similarly created synaptic-strength matrices (Figure 6B). For PC→PC connections, synaptic efficacy distributed relatively evenly across the layers (Figures 3, 4, and 5). For BCs, EPSP amplitudes were stronger in subgranular layers, especially for L5 PC→L5 BC synapses (Figure 4). In contrast, among MCs, EPSP amplitudes dominated in supragranular layers (Figure 3).

To illustrate the combined effect of connectivity and synaptic efficacy, we created path-strength matrices (Figure 6C), where path strength is the product of connectivity and EPSP amplitude.[22] Consequently, path-strength comparisons were qualitative. For PCs, this analysis highlighted the strong L4→L2/3 path. For BCs, however, L5→L5 intralaminar drive appeared to be more prominent. For MCs, L2/3→L2/3 intralaminar drive was salient. Overall, path strengths onto PCs were weaker.

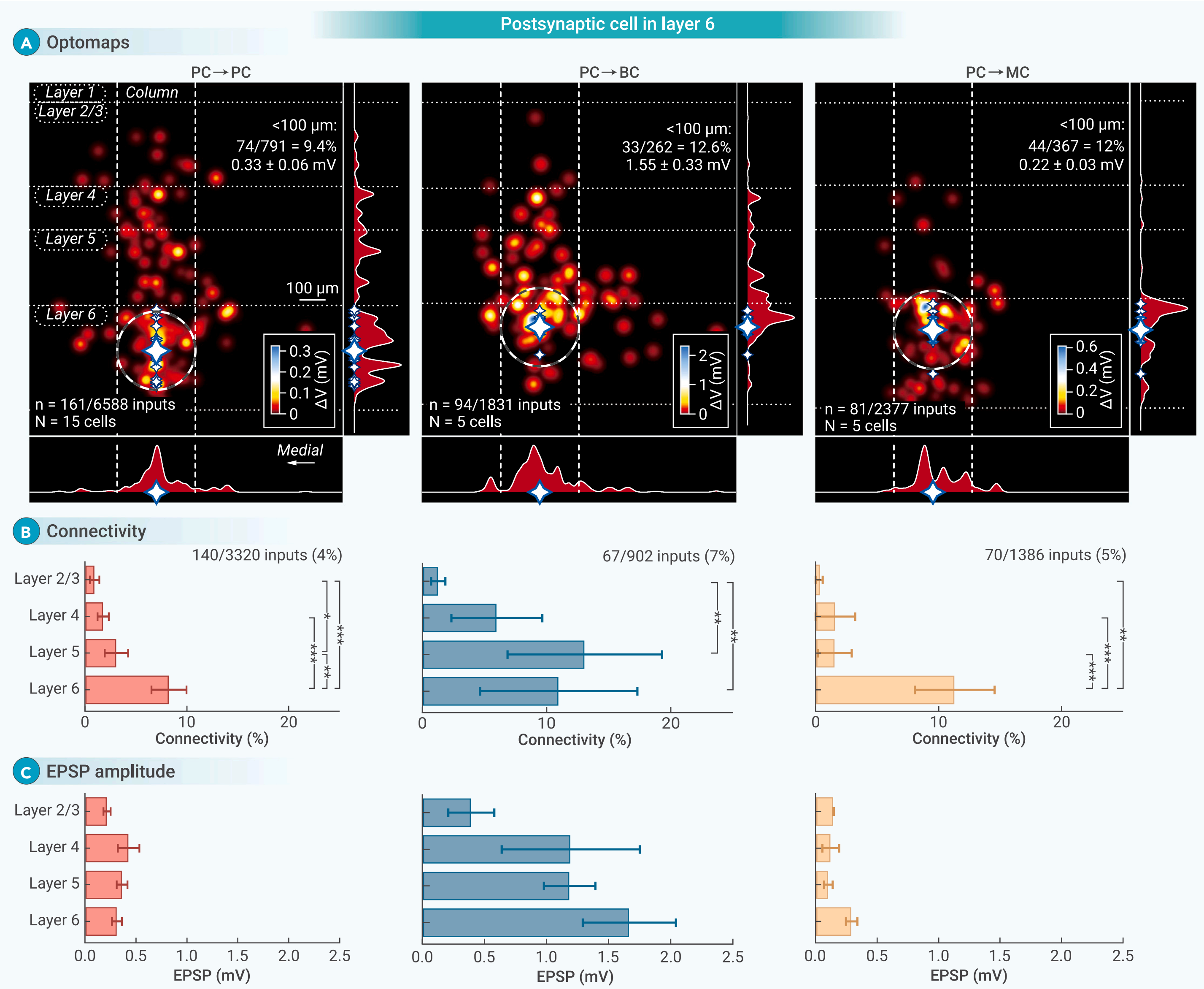

Figure 5. In L6, excitatory inputs to PCs, BCs, and MCs were chiefly from L6 (A) Synaptic input density maps for L6 PCs, BCs, and MCs. (B) L6 PCs and MCs both received more inputs from L6 than other layers. L6 BCs, however, received fewer excitatory inputs from L2/3, with an indistinguishable number of inputs from L5 and L6. BCs received more L5 inputs than PCs ($p < 0.01$) or MCs ($p < 0.001$). Connectivity depended on presynaptic layer and cell type ($p < 0.001$). (C) In L6, BCs received stronger excitation than PCs ($p < 0.01$) and MCs ($p < 0.01$). EPSP amplitudes depended on cell type ($p < 0.001$) but presynaptic layer ($p = 0.08$, interaction effect $p = 0.16$). Mean ± SEM. *$p < 0.05$, **$p < 0.01$, and ***$p < 0.001$.

In summary, excitatory microcircuit structures were target-cell specific (Figure 6D). For PCs, we reproduced the V1 canonical circuit,[4-6,53] but we found surprising differences for BCs and MCs. Finally, E→E pathways were weaker than E→I pathways.

Short-term plasticity depends on layer as well as target cell type

It is known that short-term dynamics is specific to target cell,[9] e.g., PC→MC synapses short-term facilitate but PC→PC and PC→BC connections short-term depress.[10,11,45,54] We used optomapping to explore if this principle applies to all cortical layers.

We first simultaneously optomapped excitatory inputs onto a PC, a BC, and an MC (Figure 7A), which revealed target-cell-specific synaptic dynamics (Figure 7B).[10,11,54] Quantification of short-term plasticity with the PPR revealed that synaptic responses in the PC short-term depressed, those in the BC depressed less so, and those in the MC short-term facilitated (Figure 7C). Optomapping and published paired-recording PPR values corresponded well.[45,56] Optomapping thus accurately quantifies synaptic dynamics.

To look for differences across the cortical layers, we broke down all our PPR measurements across presynaptic layer, postsynaptic layer, and postsynaptic cell type (Figure 7D). This revealed predominant short-term depression for PC→PC and PC→BC connections. However, noteworthy exceptions included L6 PC→PC and L2/3 PC→L5 BC pathways, which facilitated (Figures 7D and 7E). PC→MC synapses, however, consistently facilitated (Figures 7D and 7E).

In sum, we produced an excitatory short-term plasticitome for PCs, BCs, and MCs in developing V1,[7,26] revealing that synaptic dynamics depended on cortical layer in addition to target cell.[9] This reveals complex interactions between pre- and postsynaptic partners.

Excitation latency varies with target cell type

Due to strong facilitation[16,20,45] and a long membrane time constant[45] (Figure S5C), our 30-Hz EPSP trains temporally summated appreciably in MCs (Figure 7). Therefore, the first response, $EPSP_1$, in a train underestimated the excitation of MCs.

Therefore, we measured the peak depolarization, ΔV_{peak}, across EPSP trains and expectedly found stronger excitation of MCs (Figures S10A and S10B). ΔV_{peak} highlighted the strength of E→I over E→E connections without affecting PC→MC spatial distributions appreciably (Figures 6C and S10C). ΔV_{peak} is a useful proxy for the latency at which postsynaptic neurons tend to fire.[56] As expected,[15,16,57] BC latencies were short, and MC latencies were long (Figure S10D). Surprisingly, however, PC latencies distributed heterogeneously (Figure S10D).

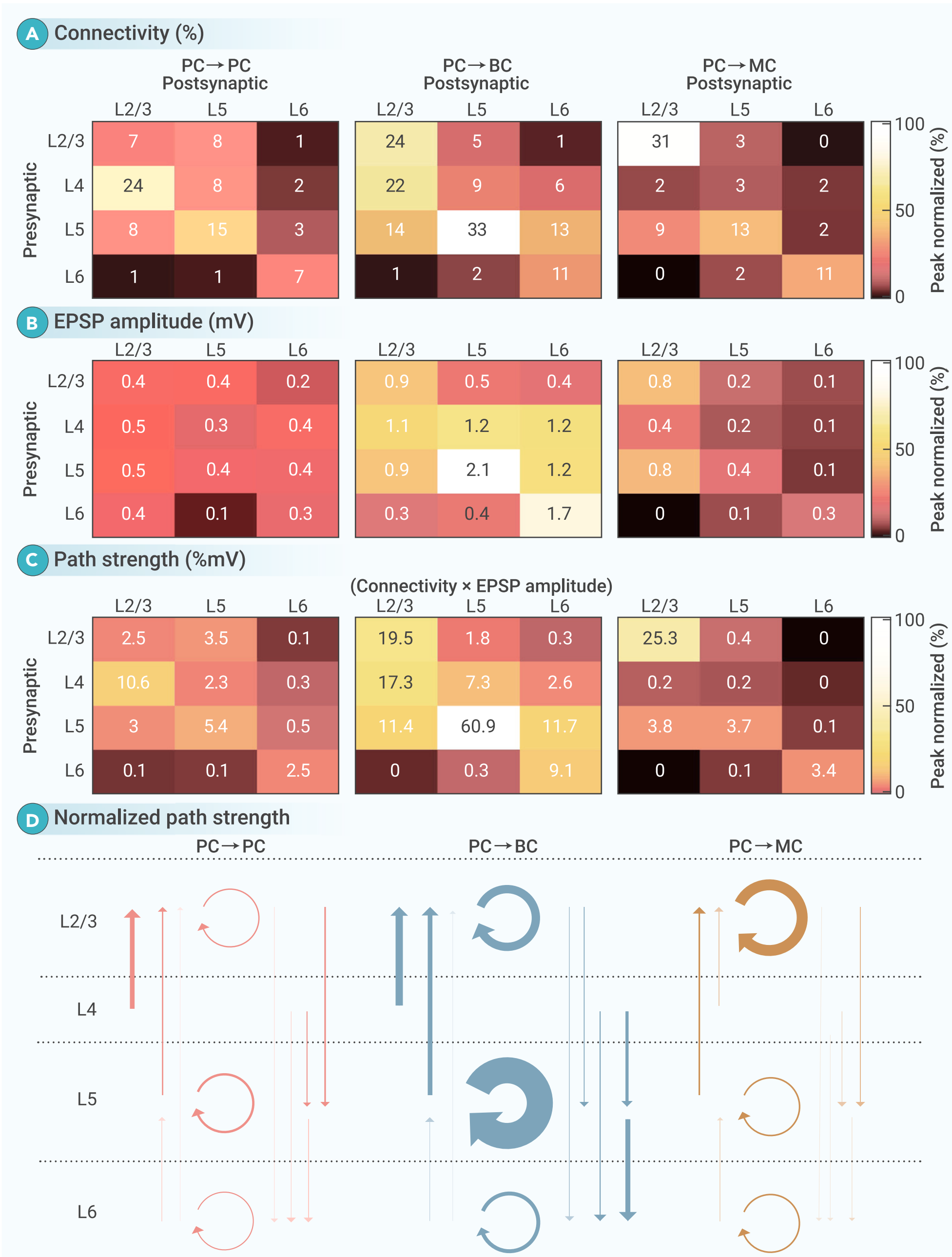

Figure 6. Excitatory circuit structure depends on target cell type (A) For PCs, L4→L2/3 connectivity was prominent. Among L5→L5 connections, PC→BC synapses stood out. For MCs, however, connectivity concentrated to L2/3→L2/3. Color code: normalized values. Cyan numbers: absolute values. Statistics: see Figures 3, 4, and 5. (B) Excitatory input strength to PCs did not depend on layer. For BCs, L5→L5 inputs were strongest, whereas for MCs, L2/3→L2/3 inputs dominated. MC matrix shows $EPSP_1$ and so does not account for PC→MC facilitation (Figure S10). Statistics: see Figures 3, 4, and 5. (C) Path strengths highlighted the strong L4→L2/3 path for PCs, but for BCs, L5→L5 dominated, and for MCs, L2/3→L2/3 was the strongest. Overall, E→E pathways were weaker than E→I pathways. (D) Arrow thickness scaled to normalized path strengths in (C) reproduced the V1 canonical circuit for PC→PC synapses.[6,53] PC→BC paths, however, were strongest in L5, and PC→MC paths dominated in L2/3.

High-order connectivity patterns in L6

Classical connectivity studies have revealed high-order connectivity patterns in L2/3 and L5.[17,23,24,58,59] We therefore examined L6 for this connectivity principle. Using Monte Carlo,[17,23,24,60,61] we revealed 4-fold overrepresentation of shared excitatory inputs for reciprocally connected, but not unconnected, PC pairs (Figure 8), thus extending this principle from L2/3 and L5 to L6. This principle furthermore holds for individual neuronal pairs.

In L2/3, excitatory inputs are overrepresented for reciprocally connected PC↔BC but not for PC-MC pairs.[58] In agreement, we found a shared-input overrepresentation for the reciprocally connected PC↔BC pair in Figure 7 (excess $\mu \pm SD = 34.3\% \pm 18\%$, $p < 0.01$, Monte Carlo, data not shown) but not for the unconnected PC-MC ($-22.4\% \pm 17\%$, $p = 0.87$). This replication validates our approach.

DISCUSSION

Here, we showcased optomapping, a high-throughput connectivity mapping method that we validated as accurate and reliable. Due to its high throughput, we were able to reveal several hitherto unappreciated principles of V1 excitatory fine structure.

The ubiquitous log-normal distribution

Many physiological and anatomical features in the brain are described by log-normal distributions,[25,62] e.g., spine size.[63] Since spine size scales with synaptic strength,[62,63] this implies that weight distributions should be similarly heavy tailed. Paired recordings have indeed revealed log-normal synaptic responses,[17,22,25,51] but because paired-recording studies pool data across cells,[17,22,51] log normality could arise as a sampling artifact because most cells are weakly driven, whereas hub neurons receive numerous strong inputs.[62] However, we found log normality in individual cells, arguing it is not a sampling artifact.

Interneurons are relatively devoid of spines,[12–14] so their weight distributions have been unclear.[25] Weight distribution log normality means few connections are strong and most weak and may underlie key capabilities such as feature encoding.[19] Consequently, PCs with similar functional preference wire together more strongly and frequently,[18] as expected from Hebbian plasticity. Accordingly, it has been suggested that log-normal weights emerge from Hebbian-like plasticity.[64,65] Since PC→BC plasticity is anti-Hebbian,[7,66,67] we speculated that interneuron weight distributions are not log normal. However, we found log normality onto both BCs and MCs, suggesting that log normality governs all excitatory synapses. It is unclear whether inhibitory synapses also distribute log normally, but pooling across cells suggests they do.[34]

Theory studies suggest that heavy-tailed distributions arise from multiplicative processes such as homeostatic, intrinsic, or structural plasticity.[64,68,69] However, spine size log normality persists in synaptic blockade,[63] suggesting that activity-dependent plasticity is not required.

Finally, we reproduced in single cells the known sparsity of cortical connectivity,[17,22,51] with mostly zero weights.[25,70] A large zero-weight fraction—i.e., potential synapses as a blank slate[71]—is key to optimal information storage.[70]

The structure of excitatory circuits

Neocortical circuits generalize across areas, repeating the same basic laminar organization.[6] Simplistically, this canonical circuit consists of an ascending path from L4 to L2/3, which then projects to L5, the output layer.[6,53] Classic studies typically explored these pathways in bulk, whereas optomapping permitted interrogation of the sublaminar structure.

PC→PC optomapping largely reproduced the canonical circuit, although we found intriguing differences compared to prior literature. Some reported that

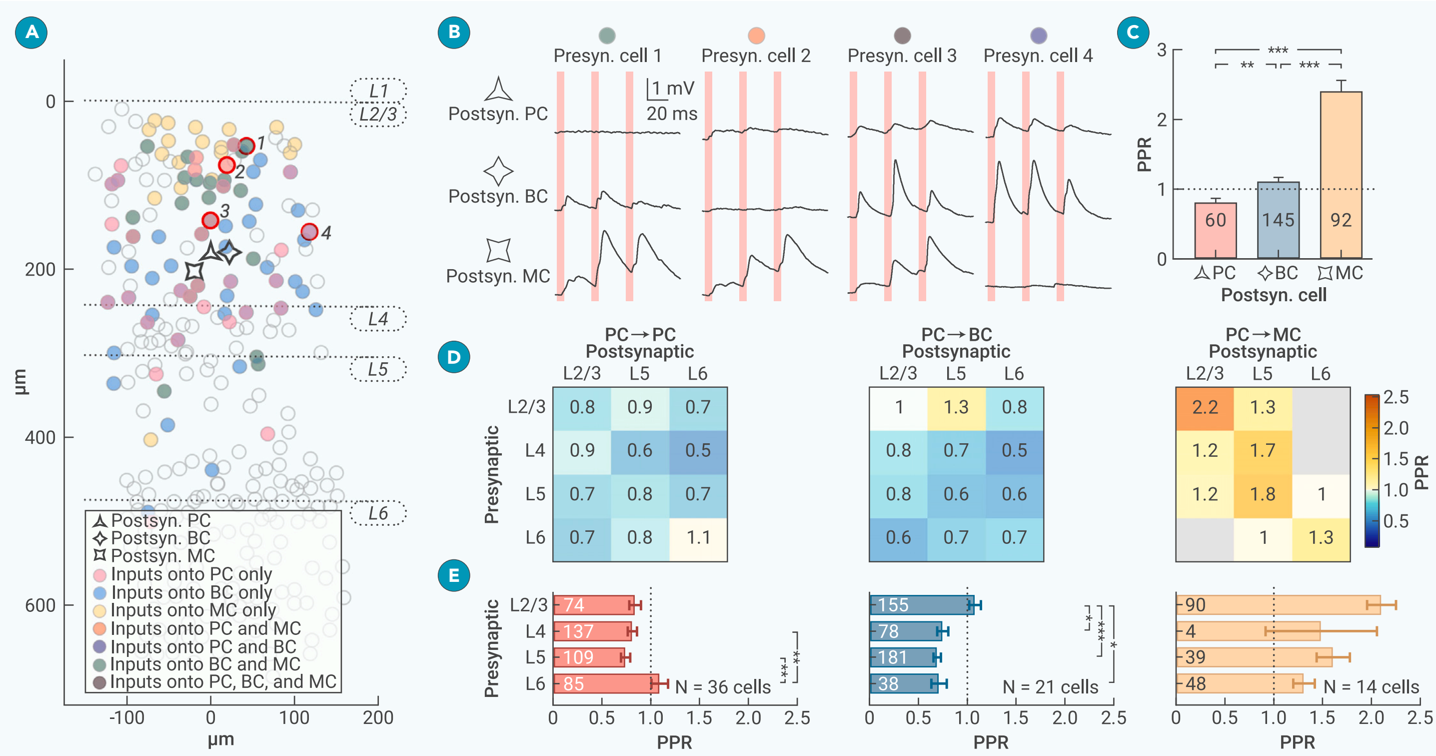

Figure 7. Synapse dynamics varied with cortical layer as well as target cell type (A) PC/BC/MC triplet recording with sample shared inputs 1–4. Out-of-plane inputs are not shown for clarity. (B) Shared inputs 1–4 facilitated onto MC but depressed onto PC and BC. Pink bars: optogenetic stimulation. (C) Across all inputs to this triplet, PC→PC short-term depressed, PC→BC depressed less so, and PC→MC facilitated. Triplet target cell thus determined synaptic dynamics.[10,11,45,54] Dashed line demarcates short-term depression from facilitation. (D) PPR analysis across all PCs, BCs, and MCs confirmed that target cell type determines synaptic dynamics.[9] However, outliers such as L6 PC→PC and L2/3 PC→L5 BC connections suggested additional dependence on layer. PPR depended on presynaptic layer and postsynaptic cell type ($p < 0.001$, LMM) but not postsynaptic layer ($p = 0.17$). For inputs from L2/3 and L5, MCs had a greater PPR than PCs ($p < 0.001$) and BCs ($p < 0.001$). For inputs from L6, BCs had a lower PPR than PCs ($p < 0.01$) and MCs ($p < 0.001$). Numbers: PPR. Gray: <3 connections. (E) Synaptic dynamics depended differentially on presynaptic layer for PCs and BCs but not MCs. Facilitation was largest in L6 for PC→PC connections but dominated in L2/3 for PC→BC synapses. Bars: PPRs pooled across postsynaptic layers. Numbers: number of inputs. Dashed line demarcates short-term depression from facilitation. Mean ± SEM. *$p < 0.05$, **$p < 0.01$, and ***$p < 0.001$.

L2/3→L5 is stronger than L2/3→L2/3,[72] but we found these paths to be indistinguishable. Like others,[34] we found prominent L5→L2/3 projections, yet these are absent from influential neocortical models,[73,74] as well as from several paired recording studies.[21,22,55] Although a known L5→L6 projection[6,53] showed up weakly, optomapping revealed a largely isolated L6, as previously shown.[20] This L6 independence may, however, be neuromodulated in the intact brain.

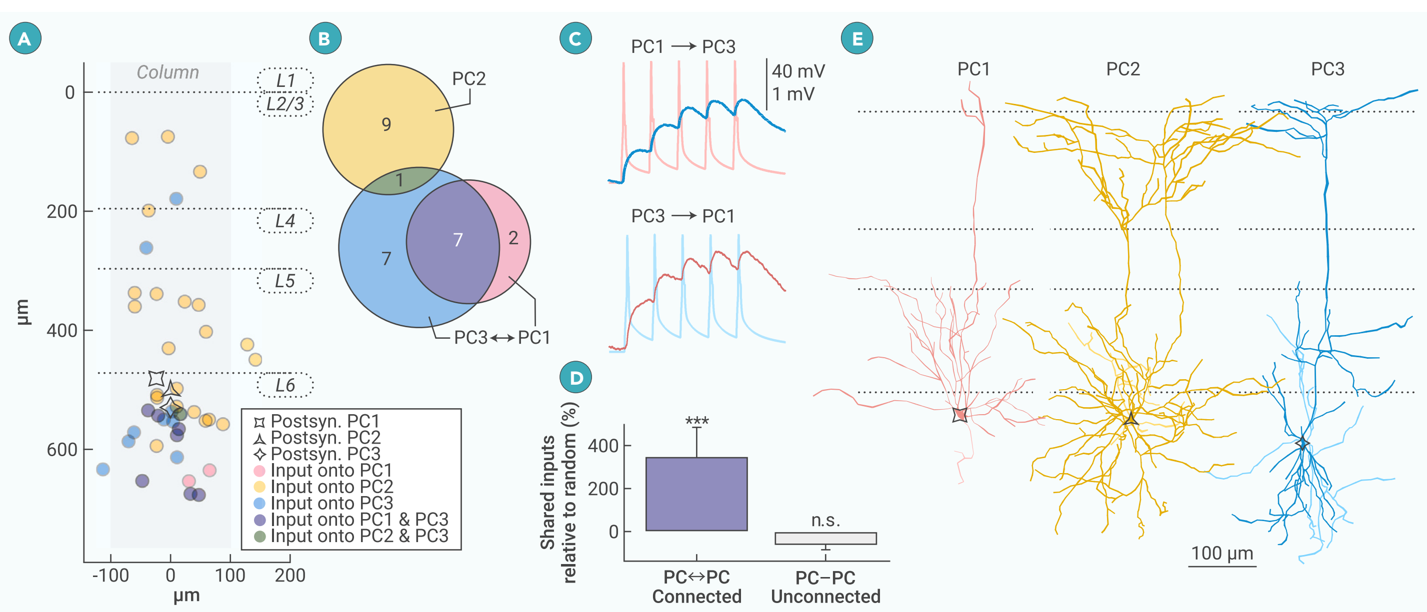

Figure 8. 4-fold overrepresentation of shared inputs onto connected L6 PCs (A) Three L6 PCs were simultaneously optomapped. Only connected inputs are shown. (B) Of the inputs in (A), several were shared by two of the patched PCs (purple). (C) PCs 1 and 3 were bidirectionally connected. EPSP traces are averages of 20 repeats. (D) Reciprocally connected PC pair shared more L6 inputs than expected from uniformly random (Monte-Carlo bootstrap). This was not true for unconnected PCs ($N = 3$ pairs pooled). (E) Three-dimensional (3D) reconstruction confirmed pyramidal cell identity. Dark: dendrite; light: axon. Mean ± SD. ***$p < 0.001$.

Key cortical interneuron types such as BCs and MCs establish functionally important recurring connectivity motifs.[15,16,57,75] We therefore considered BCs and MCs as targets in addition to PCs, which revealed striking differences. PC→BC excitation concentrated to L5, whereas PC→MC excitation dominated in L2/3, reminiscent of barrel cortex.[39] In both cases, excitation qualitatively originated from the upper half of the layer, suggesting sublaminar structuring.

Although PC→PC optomapping chiefly reproduced the canonical circuit, the layer specificity of PC→BC and PC→MC drive was surprising. MCs have been thoroughly studied in L5,[15,16,45,50,56,75] yet their L2/3 drive seems greater. The potent PC→BC drive in L5 suggests a prominent BC role in the output layer. This arrangement may promote sparse and dense coding in L2/3 and L5, respectively.[1,2]

Our study provides a snapshot of developing microcircuits, which may explain differences with studies at other ages. An interesting future direction would be to optomap across ages to reveal circuit maturation.

E→I: Denser, stronger, farther

An emerging principle was that E→I projections were denser, stronger, and farther reaching than E→E projections. This differential arrangement of E→E and E→I synapses may prevent runaway excitation in local circuits, as hyperactive PCs are promptly inhibited by strongly driven neighboring BCs and MCs.

Differential E→I and E→E spatial distributions may together provide a substrate for difference-of-Gaussian connectivity structures.[76] L2/3 I→E projections are likewise long range,[34] supporting this idea. It has long been argued that difference-of-Gaussian connectivity mediates lateral suppression in local circuits and underlies edge detection in vision.[77]

A V1 excitatory short-term plasticitome

The synapse-type specificity of short-term dynamics is well known.[9] For instance, PC→BC connections short-term depress, but PC→MC synapses facilitate, which helps BCs and MCs elicit early- and late-onset inhibition, respectively.[10,11,45,54] This principle, however, need not apply across the layers, given their distinct computational roles.[1,2,4] We therefore used optomapping to create an excitatory short-term plasticitome.[7] This replicated the known target-cell specificity of synaptic dynamics,[9] which in turn validated optomapping.

However, we additionally found stronger facilitation in L6 inputs for PCs and stronger facilitation in L2/3 inputs for BCs. To our knowledge, these cell-specific dissimilarities across the lamina have not been previously reported.[20,21] Our finding suggests that, over the course of activity bursts, E→E and E→I drive differentially varies in supra- and subgranular layers. E/I balance may thus also dynamically vary accordingly across the cortical thickness.

Factors other than synaptic short-term dynamics also determine BC and MC spiking latency, such as membrane time constant and synaptic conductance dynamics.[56] To account for such factors collectively, we also explored peak depolarization. Unsurprisingly, depolarization peaked early for BCs and late for MCs.[10,11,45,54]

However, PC peak depolarization latencies distributed heterogeneously over short EPSP bursts. PC→PC connections are well known for undergoing presynaptic forms of long-term plasticity that alter short-term synaptic dynamics.[78–80] Long-term potentiation thereby redistributes synaptic efficacy toward the beginning of EPSP bursts,[79,80] whereas long-term depression does the opposite.[78] PC→PC long-term plasticity may thus alter both the likelihood and latency of PC spiking relative to BC and MC spiking. Developing this view would require circuit computer models of long-term plasticity that include the locus of plasticity expression.[81,82]

High-order patterns of connectivity

Influential connectivity studies have revealed high-order connectivity patterns.[17,23,24,58,59] For instance, compared to unconnected L5 PC pairs, reciprocally connected L5 PCs more likely receive input from the same L2/3 PC.[23] High-order patterns are important, as they shape information processing in the brain, e.g., by binding different features of information or by creating separate information streams.[17,23,24,58,59] However, many of these studies pooled data across experiments with paired recordings.[17,23,24] They also focused on L2/3 and L5.[17,23,24,58,59]

We explored if this connectivity principle carried over to individual PC pairs in L6. We found a 4-fold overrepresentation of shared inputs onto connected L6 PCs that was not present for unconnected L6 PCs. We validated our findings by replicating prior high-order connectivity findings in L2/3.[58] The existence of high-order connectivity patterns thus extends to L6, even for individual pairs.

Patchy connectivity patterns have long been reported in L2/3 and L5[17,48,52] and have, in some cases, been attributed to the existence of different PC types,[24,83,84] and in other cases not.[23,59] Although our high-order connectivity patterns did not align with the L6 PC type, we also could not exclude this possibility.[85,86]

Caveats

Like any method, optomapping comes with caveats. We identified direct optogenetic activation of opsin-expressing postsynaptic cells as a central problem as well as approaches to mitigate it. Ideally, opsins in postsynaptic cells should be specifically blocked by drug dialysis via the recording pipette.[45,50] Such pharmacology would be a key improvement of optomapping.

As opposed to paired recordings, optomapping could not directly monitor presynaptic spiking. Even though the reliability of presynaptic spiking was high in control experiments, and even though optomapping connectivity closely matched that of paired recordings, it is possible that connected presynaptic neurons were occasionally erroneously classified as unconnected because they failed to spike. One solution would be to co-express GCaMP with the opsin to enable presynaptic spike-driven calcium imaging.[33,38,40,87–89]

The acute slice preparation suffers from undesirable severing of neuronal processes. With optomapping, it is not possible to reconstruct presynaptic neurons to evaluate their intactness. To minimize cutting artifacts, we optimized slice angle, patched and stimulated deep, and triaged data based on a threshold value for cutting angle and cell depth, but the only way to avoid this problem is to find monosynaptic connections in the intact brain, which has been done with paired recordings.[90] It would thus be interesting to adapt optomapping for *in vivo* conditions.

It is possible to identify cells with greater granularity than we did.[12-14] Future optomapping studies may classify cell types with higher resolution using, for instance, layer-specific Cre lines and patch-sequencing.[12,34,37,91] However, the use of new Cre lines requires re-characterizing the optogenetic effector.[39,88]

Outlook

The state-of-the-art approach for synapse-type-specific experimentation has long been the paired-recording technique.[17,18,20–24] This methodology, however, is difficult to learn and slow to use, leading to the throughput problem.[7,26] Consequently, relatively complete mappings of entire microcircuits have been rare.[20–22] Since circuit structure fundamentally determines circuit function,[1–3] the throughput problem has been a major impediment to progress in neuroscience research.

To solve the throughput problem, we implemented optomapping by seeking inspiration from recent advances with 2P optogenetics.[33,34,36–38,40] We validated optomapping by comparing it with paired recordings. With optomapping, we could rapidly and reliably test hundreds of candidate inputs hundreds of microns away from a patched cell, across the cortical layers and covering the entire cortical thickness, to reveal hitherto unappreciated microcircuit differences for PCs, BCs, and MCs. We estimate that optomapping is around two orders of magnitude faster than multiple patch. Additionally, without patching onto presynaptic cells and dialyzing the intracellular milieu, which is known to severely affect paired recordings in some brain regions,[92] we eliminated a subset of experimental artifact types during the measurement of synaptic events. For an even better yield, optomapping can also be combined with other approaches, such as multiple patch, pipette cleaning, and patch robots.[93–95]

Because of the throughput problem, the typical medium-sized lab has not been able to explore how local circuits differ in disease states, in genetic models, across brain areas, or across species. By solving this problem, optomapping and similar pipelines thus change what kinds of questions neuroscientists can ask. Here, we showcased an optomapping pipeline adapted from a standard 2P imaging system, as well as open-access data acquisition and analysis software. By applying optomapping to developing V1, we provided a fresh perspective on the principles that govern its excitatory fine structure.

MATERIALS AND METHODS

See the supplemental information for details.

REFERENCES

1. Harris, K.D., and Mrsic-Flogel, T.D. (2013). Cortical connectivity and sensory coding. Nature **503**: 51–58. https://doi.org/10.1038/nature12654.
2. Harris, K.D., and Shepherd, G.M.G. (2015). The neocortical circuit: themes and variations. Nat. Neurosci. **18**: 170–181. https://doi.org/10.1038/nn.3917.
3. Abbott, L.F., and Regehr, W.G. (2004). Synaptic computation. Nature **431**: 796–803. https://doi.org/10.1038/nature03010.
4. Braitenberg, V., and Schüz, A. (1998). Cortex: Statistics and Geometry of Neuronal Connectivity, 2nd Edition (Springer-Verlag Telos).
5. Shepherd, G.M. (2004). The Synaptic Organization of the Brain, 5th ed.), 5th Edition (Oxford University Press).
6. Douglas, R.J., and Martin, K.A.C. (2004). Neuronal circuits of the neocortex. Annu. Rev. Neurosci. **27**: 419–451. https://doi.org/10.1146/annurev.neuro.27.070203.144152.
7. McFarlan, A.R., Chou, C.Y.C., Watanabe, A., et al. (2023). The plasticitome of cortical interneurons. Nat. Rev. Neurosci. **24**: 80–97. https://doi.org/10.1038/s41583-022-00663-9.
8. Larsen, R.S., and Sjöström, P.J. (2015). Synapse-type-specific plasticity in local circuits. Curr. Opin. Neurobiol. **35**: 127–135. https://doi.org/10.1016/j.conb.2015.08.001.
9. Blackman, A.V., Abrahamsson, T., Costa, R.P., et al. (2013). Target Cell-Specific Short-Term Plasticity in Local Circuits. Front. Synaptic Neurosci. **5**: 11–13. https://doi.org/10.3389/fnsyn.2013.00011.
10. Reyes, A., Lujan, R., Rozov, A., et al. (1998). Target-cell-specific facilitation and depression in neocortical circuits. Nat. Neurosci. **1**: 279–285. https://doi.org/10.1038/1092.
11. Markram, H., Wang, Y., and Tsodyks, M. (1998). Differential signaling via the same axon of neocortical pyramidal neurons. Proc. Natl. Acad. Sci. USA **95**: 5323–5328.
12. Gouwens, N.W., Sorensen, S.A., Baftizadeh, F., et al. (2020). Integrated Morphoelectric and Transcriptomic Classification of Cortical GABAergic Cells. Cell **183**: 935–953.e19. https://doi.org/10.1016/j.cell.2020.09.057.
13. Markram, H., Toledo-Rodriguez, M., Wang, Y., et al. (2004). Interneurons of the neocortical inhibitory system. Nat. Rev. Neurosci. **5**: 793–807.
14. DeFelipe, J., López-Cruz, P.L., Benavides-Piccione, R., et al. (2013). New insights into the classification and nomenclature of cortical GABAergic interneurons. Nat. Rev. Neurosci. **14**: 202–216. https://doi.org/10.1038/nrn3444.
15. Silberberg, G. (2008). Polysynaptic subcircuits in the neocortex: spatial and temporal diversity. Curr. Opin. Neurobiol. **18**: 332–337. https://doi.org/10.1016/j.conb.2008.08.009.
16. Silberberg, G., and Markram, H. (2007). Disynaptic inhibition between neocortical pyramidal cells mediated by Martinotti cells. Neuron **53**: 735–746.
17. Song, S., Sjöström, P.J., Reigl, M., et al. (2005). Highly nonrandom features of synaptic connectivity in local cortical circuits. PLoS Biol. **3**: e68.
18. Ko, H., Hofer, S.B., Pichler, B., et al. (2011). Functional specificity of local synaptic connections in neocortical networks. Nature **473**: 87–91. https://doi.org/10.1038/nature09880.
19. Cossell, L., Iacaruso, M.F., Muir, D.R., et al. (2015). Functional organization of excitatory synaptic strength in primary visual cortex. Nature **518**: 399–403. https://doi.org/10.1038/nature14182.
20. Campagnola, L., Seeman, S.C., Chartrand, T., et al. (2022). Local connectivity and synaptic dynamics in mouse and human neocortex. Science **375**: eabj5861. https://doi.org/10.1126/science.abj5861.
21. Jiang, X., Shen, S., Cadwell, C.R., et al. (2015). Principles of connectivity among morphologically defined cell types in adult neocortex. Science **350**: aac9462. https://doi.org/10.1126/science.aac9462.
22. Lefort, S., Tomm, C., Floyd Sarria, J.C., et al. (2009). The excitatory neuronal network of the C2 barrel column in mouse primary somatosensory cortex. Neuron **61**: 301–316.
23. Kampa, B.M., Letzkus, J.J., and Stuart, G.J. (2006). Cortical feed-forward networks for binding different streams of sensory information. Nat. Neurosci. **9**: 1472–1473. https://doi.org/10.1038/nn1798.
24. Brown, S.P., and Hestrin, S. (2009). Intracortical circuits of pyramidal neurons reflect their long-range axonal targets. Nature **457**: 1133–1136. https://doi.org/10.1038/nature07658.
25. Barbour, B., Brunel, N., Hakim, V., et al. (2007). What can we learn from synaptic weight distributions? Trends Neurosci. **30**: 622–629. https://doi.org/10.1016/j.tins.2007.09.005.
26. Sjöström, P.J. (2021). Grand Challenge at the Frontiers of Synaptic Neuroscience. Front. Synaptic Neurosci. **13**: 748937. https://doi.org/10.3389/fnsyn.2021.748937.
27. Rickgauer, J.P., and Tank, D.W. (2009). Two-photon excitation of channelrhodopsin-2 at saturation. Proc. Natl. Acad. Sci. USA **106**: 15025–15030. https://doi.org/10.1073/pnas.0907084106.
28. Papagiakoumou, E., Anselmi, F., Bègue, A., et al. (2010). Scanless two-photon excitation of channelrhodopsin-2. Nat. Methods **7**: 848–854. https://doi.org/10.1038/nmeth.1505.
29. Packer, A.M., Peterka, D.S., Hirtz, J.J., et al. (2012). Two-photon optogenetics of dendritic spines and neural circuits. Nat. Methods **9**: 1202–1205. https://doi.org/10.1038/nmeth.2249.
30. Prakash, R., Yizhar, O., Grewe, B., et al. (2012). Two-photon optogenetic toolbox for fast inhibition, excitation and bistable modulation. Nat. Methods **9**: 1171–1179. https://doi.org/10.1038/nmeth.2215.
31. Emiliani, V., Cohen, A.E., Deisseroth, K., et al. (2015). All-Optical Interrogation of Neural Circuits. J. Neurosci. **35**: 13917–13926. https://doi.org/10.1523/JNEUROSCI.2916-15.2015.
32. Shemesh, O.A., Tanese, D., Zampini, V., et al. (2017). Temporally precise single-cell-resolution optogenetics. Nat. Neurosci. **20**: 1796–1806. https://doi.org/10.1038/s41593-017-0018-8.
33. Mardinly, A.R., Oldenburg, I.A., Pégard, N.C., et al. (2018). Precise multimodal optical control of neural ensemble activity. Nat. Neurosci. **21**: 881–893. https://doi.org/10.1038/s41593-018-0139-8.
34. Hage, T.A., Bosma-Moody, A., Baker, C.A., et al. (2022). Synaptic connectivity to L2/3 of primary visual cortex measured by two-photon optogenetic stimulation. Elife **11**: e71103. https://doi.org/10.7554/eLife.71103.
35. Baker, C.A., Elyada, Y.M., Parra, A., et al. (2016). Cellular resolution circuit mapping with temporal-focused excitation of soma-targeted channelrhodopsin. Elife **5**: e14193. https://doi.org/10.7554/eLife.14193.
36. Izquierdo-Serra, M., Hirtz, J.J., Shababo, B., et al. (2018). Two-Photon Optogenetic Mapping of Excitatory Synaptic Connectivity and Strength. iScience **8**: 15–28.
37. Seeman, S.C., Campagnola, L., Davoudian, P.A., et al. (2018). Sparse recurrent excitatory connectivity in the microcircuit of the adult mouse and human cortex. Elife **7**: e37349. https://doi.org/10.7554/eLife.37349.
38. Chettih, S.N., and Harvey, C.D. (2019). Single-neuron perturbations reveal feature-specific competition in V1. Nature **567**: 334–340. https://doi.org/10.1038/s41586-019-0997-6.
39. Naka, A., Veit, J., Shababo, B., et al. (2019). Complementary networks of cortical somatostatin interneurons enforce layer specific control. Elife **8**: e43696. https://doi.org/10.7554/eLife.43696.
40. Printz, Y., Patil, P., Mahn, M., et al. (2023). Determinants of functional synaptic connectivity among amygdala-projecting prefrontal cortical neurons in male mice. Nat. Commun. **14**: 1667. https://doi.org/10.1038/s41467-023-37318-x.
41. Kim, J.Y., Grunke, S.D., Levites, Y., et al. (2014). Intracerebroventricular viral injection of the neonatal mouse brain for persistent and widespread neuronal transduction. J. Vis. Exp. 51863. https://doi.org/10.3791/51863.
42. Gorski, J.A., Talley, T., Qiu, M., et al. (2002). Cortical excitatory neurons and glia, but not GABAergic neurons, are produced in the Emx1-expressing lineage. J. Neurosci. **22**: 6309–6314.
43. Dimidschstein, J., Chen, Q., Tremblay, R., et al. (2016). A viral strategy for targeting and manipulating interneurons across vertebrate species. Nat. Neurosci. **19**: 1743–1749. https://doi.org/10.1038/nn.4430.
44. Packer, A.M., Russell, L.E., and Dalgleish, H.W.P. (2015). Simultaneous all-optical manipulation and recording of neural circuit activity with cellular resolution *in vivo*. Nat. Methods **12**: 140–146. https://doi.org/10.1038/nmeth.3217.
45. Buchanan, K.A., Blackman, A.V., Moreau, A.W., et al. (2012). Target-Specific Expression of Presynaptic NMDA Receptors in Neocortical Microcircuits. Neuron **75**: 451–466. https://doi.org/10.1016/j.neuron.2012.06.017.
46. Lein, E.S., Hawrylycz, M.J., Ao, N., et al. (2007). Genome-wide atlas of gene expression in the adult mouse brain. Nature **445**: 168–176. https://doi.org/10.1038/nature05453.
47. Paxinos, G. (2001). In The Mouse Brain in Stereotaxic Coordinates, 2nd ed., K.B.J. Franklin, ed. (Academic).
48. Holmgren, C., Harkany, T., Svennenfors, B., et al. (2003). Pyramidal cell communication within local networks in layer 2/3 of rat neocortex. J. Physiol. **551**: 139–153.
49. Abrahamsson, T., Chou, C.Y.C., Li, S.Y., et al. (2017). Differential Regulation of Evoked and Spontaneous Release by Presynaptic NMDA Receptors. Neuron **96**: 839–855.e5. https://doi.org/10.1016/j.neuron.2017.09.030.
50. Wong, H.H., Watt, A.J., and Sjöström, P.J. (2023). Synapse-specific burst coding sustained by local axonal translation. Neuron **112**: 264–276.e6. https://doi.org/10.1016/j.neuron.2023.10.011.
51. Feldmeyer, D., Lübke, J., Silver, R.A., et al. (2002). Synaptic connections between layer 4 spiny neurone-layer 2/3 pyramidal cell pairs in juvenile rat barrel cortex: physiology and anatomy of interlaminar signalling within a cortical column. J. Physiol. **538**: 803–822.
52. Perin, R., Berger, T.K., and Markram, H. (2011). A synaptic organizing principle for cortical neuronal groups. Proc. Natl. Acad. Sci. USA **108**: 5419–5424. https://doi.org/10.1073/pnas.1016051108.
53. Burkhalter, A. (1989). Intrinsic connections of rat primary visual cortex: laminar organization of axonal projections. J. Comp. Neurol. **279**: 171–186. https://doi.org/10.1002/cne.902790202.
54. Kim, M.H., Radaelli, C., Thomsen, E.R., et al. (2023). Target cell-specific synaptic dynamics of excitatory to inhibitory neuron connections in supragranular layers of human neocortex. Elife **12**: e81863. https://doi.org/10.7554/eLife.81863.
55. Reyes, A., and Sakmann, B. (1999). Developmental switch in the short-term modification of unitary EPSPs evoked in layer 2/3 and layer 5 pyramidal neurons of rat neocortex. J. Neurosci. **19**: 3827–3835.
56. Lalanne, T., Oyrer, J., Mancino, A., et al. (2016). Synapse-specific expression of calcium-permeable AMPA receptors in neocortical layer 5. J. Physiol. **594**: 837–861. https://doi.org/10.1113/JP271394.
57. Pouille, F., and Scanziani, M. (2001). Enforcement of temporal fidelity in pyramidal cells by somatic feed-forward inhibition. Science **293**: 1159–1163.
58. Yoshimura, Y., and Callaway, E.M. (2005). Fine-scale specificity of cortical networks depends on inhibitory cell type and connectivity. Nat. Neurosci. **8**: 1552–1559. https://doi.org/10.1038/nn1565.
59. Yoshimura, Y., Dantzker, J.L.M., and Callaway, E.M. (2005). Excitatory cortical neurons form fine-scale functional networks. Nature **433**: 868–873. https://doi.org/10.1038/nature03252.
60. Efron, B. (1979). Bootstrap Methods: Another Look at the Jackknife. Ann. Stat. **7**: 1–26.
61. Gruver, K.M., Jiao, J.W.Y., Fields, E., et al. (2024). Structured connectivity in the output of the cerebellar cortex. Nat. Commun. **15**: 5563. https://doi.org/10.1038/s41467-024-49339-1.

62. Buzsaki, G., and Mizuseki, K. (2014). The log-dynamic brain: how skewed distributions affect network operations. Nat. Rev. Neurosci. ***15***: 264–278. https://doi.org/10.1038/nrn3687.
63. Rößler, N., Jungenitz, T., Sigler, A., et al. (2023). Skewed distribution of spines is independent of presynaptic transmitter release and synaptic plasticity, and emerges early during adult neurogenesis. Open Biol. ***13***: 230063. https://doi.org/10.1098/rsob.230063.
64. Scheler, G. (2017). Logarithmic distributions prove that intrinsic learning is Hebbian. F1000Res. ***6***: 1222. https://doi.org/10.12688/f1000research.12130.2.
65. Lynn, C.W., Holmes, C.M., and Palmer, S.E. (2024). Heavy-tailed neuronal connectivity arises from Hebbian self-organization. Nat. Phys. ***20***: 484–491. https://doi.org/10.1038/s41567-023-02332-9.
66. Camiré, O., and Topolnik, L. (2014). Dendritic calcium nonlinearities switch the direction of synaptic plasticity in fast-spiking interneurons. J. Neurosci. ***34***: 3864–3877. https://doi.org/10.1523/JNEUROSCI.2253-13.2014.
67. Lamsa, K.P., Heeroma, J.H., Somogyi, P., et al. (2007). Anti-Hebbian long-term potentiation in the hippocampal feedback inhibitory circuit. Science ***315***: 1262–1266.
68. Loewenstein, Y., Kuras, A., and Rumpel, S. (2011). Multiplicative dynamics underlie the emergence of the log-normal distribution of spine sizes in the neocortex *in vivo*. J. Neurosci. ***31***: 9481–9488. https://doi.org/10.1523/JNEUROSCI.6130-10.2011.
69. Zheng, P., Dimitrakakis, C., and Triesch, J. (2013). Network self-organization explains the statistics and dynamics of synaptic connection strengths in cortex. PLoS Comput. Biol. ***9***: e1002848. https://doi.org/10.1371/journal.pcbi.1002848.
70. Brunel, N. (2016). Is cortical connectivity optimized for storing information? Nat. Neurosci. ***19***: 749–755. https://doi.org/10.1038/nn.4286.
71. Kalisman, N., Silberberg, G., and Markram, H. (2005). The neocortical microcircuit as a tabula rasa. Proc. Natl. Acad. Sci. USA ***102***: 880–885.
72. Petreanu, L., Huber, D., Sobczyk, A., et al. (2007). Channelrhodopsin-2-assisted circuit mapping of long-range callosal projections. Nat. Neurosci. ***10***: 663–668. https://doi.org/10.1038/nn1891.
73. Haeusler, S., and Maass, W. (2007). A statistical analysis of information-processing properties of lamina-specific cortical microcircuit models. Cerebr. Cortex ***17***: 149–162. https://doi.org/10.1093/cercor/bhj132.
74. Bastos, A.M., Usrey, W.M., Adams, R.A., et al. (2012). Canonical microcircuits for predictive coding. Neuron ***76***: 695–711.
75. Berger, T.K., Silberberg, G., Perin, R., et al. (2010). Brief bursts self-inhibit and correlate the pyramidal network. PLoS Biol. ***8***: e1000473. https://doi.org/10.1371/journal.pbio.1000473.
76. Smith, G.B., Hein, B., Whitney, D.E., et al. (2018). Distributed network interactions and their emergence in developing neocortex. Nat. Neurosci. ***21***: 1600–1608. https://doi.org/10.1038/s41593-018-0247-5.
77. Marr, D., and Hildreth, E. (1980). Theory of edge detection. Proc. R. Soc. Lond. B Biol. Sci. ***207***: 187–217. https://doi.org/10.1098/rspb.1980.0020.
78. Sjöström, P.J., Turrigiano, G.G., and Nelson, S.B. (2003). Neocortical LTD via coincident activation of presynaptic NMDA and cannabinoid receptors. Neuron ***39***: 641–654.
79. Sjöström, P.J., Turrigiano, G.G., and Nelson, S.B. (2007). Multiple forms of long-term plasticity at unitary neocortical layer 5 synapses. Neuropharmacology ***52***: 176–184.
80. Markram, H., and Tsodyks, M. (1996). Redistribution of synaptic efficacy between neocortical pyramidal neurons. Nature ***382***: 807–810.
81. Mizusaki, B.E.P., Li, S.S.Y., Costa, R.P., et al. (2021). Pre- and postsynaptically expressed spike-timing-dependent plasticity contribute differentially to neuronal learning. Preprint at bioRxiv. https://doi.org/10.1101/2021.09.01.458493.
82. Costa, R.P., Mizusaki, B.E.P., Sjöström, P.J., et al. (2017). Functional consequences of pre- and postsynaptic expression of synaptic plasticity. Phil. Trans. Biol. Sci. ***372***: 20160153. https://doi.org/10.1098/rstb.2016.0153.
83. Kim, E.J., Juavinett, A.L., Kyubwa, E.M., et al. (2015). Three Types of Cortical Layer 5 Neurons That Differ in Brain-wide Connectivity and Function. Neuron ***88***: 1253–1267. https://doi.org/10.1016/j.neuron.2015.11.002.
84. Kim, M.H., Znamenskiy, P., Iacaruso, M.F., et al. (2018). Segregated Subnetworks of Intracortical Projection Neurons in Primary Visual Cortex. Neuron ***100***: 1313–1321.e6. https://doi.org/10.1016/j.neuron.2018.10.023.
85. Zarrinpar, A., and Callaway, E.M. (2006). Local connections to specific types of layer 6 neurons in the rat visual cortex. J. Neurophysiol. ***95***: 1751–1761. https://doi.org/10.1152/jn.00974.2005.
86. Cotel, F., Fletcher, L.N., Kalita-de Croft, S., et al. (2018). Cell Class-Dependent Intracortical Connectivity and Output Dynamics of Layer 6 Projection Neurons of the Rat Primary Visual Cortex. Cerebr. Cortex ***28***: 2340–2350. https://doi.org/10.1093/cercor/bhx134.
87. Marshel, J.H., Kim, Y.S., Machado, T.A., et al. (2019). Cortical layer-specific critical dynamics triggering perception. Science ***365***: eaaw5202. https://doi.org/10.1126/science.aaw5202.
88. Bounds, H.A., Sadahiro, M., Hendricks, W.D., et al. (2023). All-optical recreation of naturalistic neural activity with a multifunctional transgenic reporter mouse. Cell Rep. ***42***: 112909. https://doi.org/10.1016/j.celrep.2023.112909.
89. Oldenburg, I.A., Hendricks, W.D., Handy, G., et al. (2024). The logic of recurrent circuits in the primary visual cortex. Nat. Neurosci. ***27***: 137–147. https://doi.org/10.1038/s41593-023-01510-5.
90. Jouhanneau, J.S., and Poulet, J.F.A. (2019). Multiple Two-Photon Targeted Whole-Cell Patch-Clamp Recordings From Monosynaptically Connected Neurons *in vivo*. Front. Synaptic Neurosci. ***11***: 15. https://doi.org/10.3389/fnsyn.2019.00015.
91. Lee, B.R., Budzillo, A., Hadley, K., et al. (2021). Scaled, high fidelity electrophysiological, morphological, and transcriptomic cell characterization. Elife ***10***: e65482. https://doi.org/10.7554/eLife.65482.
92. Diana, M.A., and Marty, A. (2003). Characterization of depolarization-induced suppression of inhibition using paired interneuron–Purkinje cell recordings. J Neurosci ***23***: 5906–5918.
93. Annecchino, L.A., Morris, A.R., Copeland, C.S., et al. (2017). Robotic Automation of In Vivo Two-Photon Targeted Whole-Cell Patch-Clamp Electrophysiology. Neuron ***95***: 1048–1055.e3. https://doi.org/10.1016/j.neuron.2017.08.018.
94. Suk, H.J., van Welie, I., Kodandaramaiah, S.B., et al. (2017). Closed-Loop Real-Time Imaging Enables Fully Automated Cell-Targeted Patch-Clamp Neural Recording In Vivo. Neuron ***95***: 1037–1047.e11. https://doi.org/10.1016/j.neuron.2017.08.011.
95. Peng, Y., Mittermaier, F.X., Planert, H., et al. (2019). High-throughput microcircuit analysis of individual human brains through next-generation multineuron patch-clamp. Elife ***8***: e48178. https://doi.org/10.7554/eLife.48178.

ACKNOWLEDGMENTS

We thank Alanna Watt, Charles Bourque, Keith Murai, Aparna Suvrathan, Arjun Krishnaswamy, Ed Ruthazer, Jonathan Britt, Jon Sakata, Amanda McFarlan, Haley Renault, Shawniya Alageswaran, Connor O'Donnell, Alex Zhao, Christopher Salmon, W. Todd Farmer, Riccardo Beltramo, Or Shemesh, Yoaz Printz, Ofer Yizhar, Hillel Adesnik, Adam Packer, Karl Deisseroth, and Sjöström lab members. C.Y.C.C. won Max E. Binz, HBHL, NSERC CGS D 534171-2019, FRQNT B2X 275075, and the Ann and Richard Sievers Neuroscience Award. H.H.W.W. was supported by CIHR 295104, HBHL, FRQS 259572, and RBIQ 35450 fellowships. C.G. won NSERC USRA, FRQNT BPC, RI-MUHC, FRQS, and CIHR CGS-M studentships. K.E.B. was funded by IBRO. T.A.L. won the NSERC USRA. P.J.S. is funded by the MGH Foundation; CFI LOF 28331; CIHR PGs 156223, 191969, and 191997; FRSQ CB 254033; and NSERC DG/DAS 2024-06712, 2017-04730, and 2017-507818.

AUTHOR CONTRIBUTIONS

Conceptualization, C.Y.C.C. and P.J.S.; methodology, C.Y.C.C. and P.J.S.; investigation – optomapping, C.Y.C.C.; investigation – quadruple patch clamp, C.Y.C.C. and H.H.W.W.; investigation – neuronal reconstructions, C.Y.C.C., K.E.B., C.G., C.H., J.J., T.K., V.Y.L., T.A.L., and V.C.W.; custom software, P.J.S.; formal analysis, C.Y.C.C. and P.J.S.; writing – original draft, C.Y.C.C. and P.J.S.; writing – review & editing, C.Y.C.C., H.H.W.W., and P.J.S.; funding acquisition, C.Y.C.C., H.H.W.W., and P.J.S; supervision, P.J.S.

DECLARATION OF INTERESTS

The funders had no role in study design, data collection and interpretation, or the decision to submit the work for publication.

SUPPLEMENTAL INFORMATION

It can be found online at https://doi.org/10.1016/j.xinn.2024.100735.

LEAD CONTACT WEBSITE

https://plasticity.muhc.mcgill.ca/
https://www.mcgill.ca/crn/research/sjostrom